Author(s): Deng, Guocheng; Malola, Sami; Yuan, Peng; Liu, Xianhu; Teo, Boon K.; Häkkinen, Hannu; Zheng, Nanfeng

Title: Enhanced Surface Ligands Reactivity of Metal Clusters by Bulky Ligands for Controlling Optical and Chiral Properties

Year: 2021

Version: Accepted version (Final draft)

Please cite the original version:

Deng, G., Malola, S., Yuan, P., Liu, X., Teo, B. K., Häkkinen, H., & Zheng, N. (2021). Enhanced Surface Ligands Reactivity of Metal Clusters by Bulky Ligands for Controlling Optical and Chiral Properties. Angewandte Chemie, 60(23), 12897-12903. https://doi.org/10.1002/anie.202101141

A Journal of the Gesellschaft Deutscher Chemiker

Angewandte International Edition GDCh Chemie

www.angewandte.org

Accepted Article

Title: Enhanced Surface Ligands Reactivity of Metal Clusters by Bulky Ligands for Controlling Optical and Chiral Properties

Authors: Guocheng Deng, Sami Malola, Peng Yuan, Xianhu Liu, Boon K. Teo, Hannu Häkkinen, and Nanfeng Zheng

To be cited as: *Angew. Chem. Int. Ed.* 10.1002/anie.202101141

Link to VoR: https://doi.org/10.1002/anie.202101141

WILEY-VCH

10.1002/anie.202101141

WILEY-VCH

RESEARCH ARTICLE

Enhanced Surface Ligands Reactivity of Metal Clusters by Bulky Ligands for Controlling Optical and Chiral Properties

Guocheng Deng,[a] Sami Malola,[b] Peng Yuan,[a] Xianhu Liu,[a] Boon K. Teo,[a] Hannu Häkkinen*[b] and Nanfeng Zheng*[a]

[a] G. C. Deng, P. Yuan, Dr. X. H. Liu, Prof. B. K. Teo, Prof. N. F. Zheng
State Key Laboratory for Physical Chemistry of Solid Surfaces, Collaborative Innovation Center of Chemistry for Energy Materials, and National & Local Joint Engineering Research Center of Preparation Technology of Nanomaterials, College of Chemistry and Chemical Engineering, Xiamen University
Xiamen 361005, China
E-mail: nfzheng@xmu.edu.cn

[b] Dr. S. Malola, Prof. H. Häkkinen
Departments of Physics and Chemistry, Nanoscience Center, University of Jyväskylä
FI-40014 Jyväskylä, Finland
E-mail: hannu.j.hakkinen@jyu.fi

Supporting information for this article is given via a link at the end of the document.

Abstract: Surface ligands play critical roles in determining the surface properties of metal clusters. However, modulating the properties and controlling the surface structure of clusters through surface-capping agent displacement remain a challenge. In this work, a silver cluster, $[Ag_{14}(SPh(CF_3)_2)_{12}(PPh_3)_4(DMF)_4]$ (**Ag_{14}-DMF**, where $HSPh(CF_3)_2$ is 3,5-bis(trifluoromethyl)benzenethiol, PPh_3 is triphenylphosphine and DMF is N,N-Dimethylformamide), with weakly coordinated DMF ligands on the surface silver sites, was synthesized by using a mixed ligands strategy (bulky thiolates, phosphines and small solvents). The as-prepared **Ag_{14}-DMF** is a racemic mixture of chiral molecules. Owing to the unusually high surface reactivity of **Ag_{14}-DMF**, the surface ligands are labile, easily dissociated or exchanged by other ligands. Based on the enhanced surface reactivity, easy modulation on the optical properties of **Ag_{14}** by reversible "on-off" DMF ligation was realized. The mechanism was unraveled and rationalized by density functional theory (DFT) calculations. When chiral amines were introduced to as-prepared products, all eight surface ligands were replaced by amines and the racemic **Ag_{14}** clusters were converted to optically pure homochiral **Ag_{14}** clusters as evidenced by circular dichroism (CD) activity and single-crystal X-ray diffraction (SCXRD). This work not only provides a new insight as to how to modulate the optical properties of metal clusters, but also unveils an efficient way to obtain atomically precise homochiral clusters for specific applications.

Introduction

Metal clusters are deemed as ideal miniatures of organic-capped metal nanoparticles due to their intermediate size regime that bridges the molecules and plasmonic nanoparticles.[1] To date, numerous chemical means have been established for modulating the size, shape and composition of metal nanoclusters for specific applications.[2] Surface-capping agent is one of the most important factors in determining the chemical or physical properties of nanoclusters/nanoparticles. Many studies have revealed that surface ligands on nanoparticles can not only introduce steric effects, but also modulate the surface electronic state of the nanoparticles, which are important for catalysis.[3] For instance, bulky ligands (e.g., thiolates, N-heterocylic carbenes) have been demonstrated to readily promote the surface reactivity of nanoclusters, thereby helping to achieve rapid ligands exchange as well as high catalysis performance.[4] However, modulating the electronic structure of clusters without altering their atomic structures through ligand engineering is still an elusive and unmanageable target.

On the other hand, chiral metal clusters have attracted broad research interest in recent years due to their potential applications, such as asymmetric catalysis, chiral sensing.[5] However, most of the chiral clusters were synthesized in the form of racemic mixtures.[6] Although many efforts (chiral HPLC columns, supramolecular assembly strategy with α-cyclodextrin) have been made to enantioseparate the racemic mixtures, it is still a challenge to produce optically pure clusters through these methods.[7] In order to realize 100% optical purity, chiral ligands are devised and using as protected group for enantioselective synthesis of chiral metal clusters.[8] However, until now, only a few chiral phosphine, alkynyl or thiolate ligands are available for preparing chiral metal clusters.[8a-d, 8f, 9] Thus, devising a general methodology for obtaining chiral clusters with optical purity by commonly used chiral ligands is urgently needed.

Though most of the commonly used thiolate or alkynyl ligands possess strong coordination ability to metals, weakly coordinating ligands (such as CrO_4^-, SbF_6^-) can also be introduced to metal nanoclusters through rational design.[10] Taking advantage of these weakly coordinated sites, functional or chiral ligands have been introduced on the Ag(I) clusters.[11] It occurs to us that a highly promising way to realize controls of properties of clusters is through surface modification via weakly coordinated sites which possess high reactivities. Inspired by this, we have used a mixed ligands strategy (with bulky thiolates, phosphines and small solvent ligands), to synthesize a chiral silver cluster, $[Ag_{14}(SPh(CF_3)_2)_{12}(PPh_3)_4(DMF)_4]$ (abbreviated hereafter as **Ag_{14}-DMF**). Surprisingly, this molecular cluster has unusually high surface reactivities. Furthermore, we show that optical properties and chirality can be modulated by rational design of the solvent conditions and the surface substitution chemistry of these clusters.

10.1002/anie.202101141

Results and Discussion

Synthesis and Characterization of Ag_{14}-DMF. The **Ag_{14}-DMF** cluster was synthesized by reducing a mixture of Ag compound, PPh_3 and $(CF_3)_2PhSH$ with $NaBH_4$ in a mixture of three different solvents of DMF, dichloromethane (DCM) and water (see experimental section for more details). Yellow single crystals were grown by diffusion with hexane after ten days. (Figure S1) Single-crystal X-ray diffraction (SCXRD) revealed that **Ag_{14}-DMF** is a racemate which crystallized in *C*2/c space group and the unit cell comprises a pair (Z=2) of enantiomers (Table S1 and Figure S2). No counter ions were found in the unit cell, which means this cluster belongs to two electron superatomic clusters (14-12=2). The structure of **Ag_{14}-DMF** is similar to the previously reported two electron superatomic cluster, $[Ag_{14}(SC_6H_3F_2)_{12}(PPh_3)_8]$ ($HSC_6H_3F_2$ = 3,4-difluoro-benzenethiol),[12] except that four of the phosphine ligands were replaced by DMF solvent molecules (Figure S3). As shown in Figure 1a and b, the 14 silver atoms of the **Ag_{14}-DMF** form a twisted *fcc* structure. Each edge of the twisted cube is coordinated by a thiolate ligand. Four PPh_3 and four DMF ligands coordinate to the eight corners of the twisted cube.

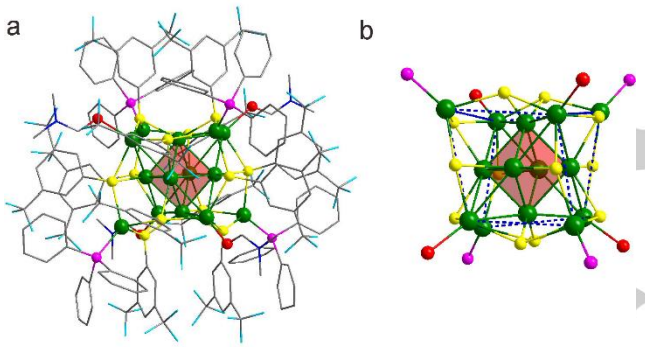

Figure 1. a) Molecular structure of **Ag_{14}-DMF**. b) Core structure of **Ag_{14}-DMF**. Color legend: green sphere, Ag; yellow sphere, S; pink sphere, P; red sphere, O; blue sphere, N; sky blue sphere, F; grey sphere, C. All hydrogen atoms are omitted for clarity.[15]

A detailed analysis of the structures revealed that, due to the steric hindrance of the bulky thiolate ligands (the percent buried volume ($\%V_{bur}$) of $HSPh(CF_3)_2$ and $HSC_6H_3F_2$ have been calculated by SambVca (Salerno molecular buried volume calculation) software[13], the result for $HSPh(CF_3)_2$ was 15.6%, and for $HSC_6H_3F_2$ was 12.0%.), it is virtually impossible for the cluster to accommodate eight PPh_3 ligands as in the case of $[Ag_{14}(SC_6H_3F_2)_{12}(PPh_3)_8]$ cluster (Figure S3). Instead, only four PPh_3 ligands are observed on each **Ag_{14}-DMF**. The four PPh_3 ligands are arranged in a tetrahedral array (with an idealized T_d point-group symmetry). The remaining four vertices of the cube are occupied by four DMF molecules. Despite this arrangement, there remains severe steric hindrance between the twelve bulky thiolate ligands and the four PPh_3 ligands. As a result, the four silver atoms coordinated with PPh_3 are farther from the octahedral Ag_6^{4+} core with an average (nonbonding) Ag-Ag distance of 3.88 Å (Figure S4a). In contrast, the four silver atoms coordinated with the small DMF molecules are closer to the Ag_6^{4+} core, with an average bond length of 3.05 Å (Figure S4b and Table S2). Both of these Ag-Ag distances are significantly longer than the average bond length of 2.85 Å within the octahedral Ag_6^{4+} core.

Interestingly, the crystals of **Ag_{14}-DMF** exhibits distinctly different colors when dissolved in different solvents. As shown in Figure 2a, pink, orange and light yellow colored solutions were obtained when crystals of **Ag_{14}-DMF** were dissolved in diethyl ether, methanol and DMF solution, respectively. The UV-vis spectra of **Ag_{14}-DMF** in commonly used solvents are shown in Figure 2b and S5. When the clusters were dissolved in diethyl ether, DCM, toluene and ethanol solution, two strong bands at 450 and 527 nm and a shoulder peak at 375 nm were observed. In methanol, a strong peak at 380 nm and a shoulder peak at 520 nm were observed. However, only one strong band at around 375 nm appeared in the UV-vis spectra of the clusters in DMF, DMSO and pyridine (Py). Moreover, the **Ag_{14}-DMF** in different solvents also showed different fluorescent spectra at room temperature. While **Ag_{14}-DMF** in diethyl ether showed a red emission around 640 nm, two emission peaks at 570 and 620 nm were observed for the clusters dissolved in methanol. Yellow emission with peak at around 560 nm was observed for the DMF solution of **Ag_{14}-DMF** (Figure S6). Hence, the common solvents studied here can be qualitatively classified into three categories based on their different relative coordination abilities: (a) no (or very weak) coordination ability such as diethyl ether, DCM, toluene and ethanol; (b) weak coordination capability such as methanol; and (c) relatively strong coordination power such as DMF, DMSO and pyridine. Based on this analysis, we reason that the different colors exhibited by **Ag_{14}-DMF** in different solvents may be due to the weak bonding between DMF ligands and surface Ag atoms. When dissolved in solvents with low coordination abilities (such as diethyl ether and methanol), DMF molecules would dissociate from the cluster (as in ether or DCM) or replaced by the solvent molecules (as in methanol), thereby altering the optical properties of the **Ag_{14}** cluster and causing the color change from yellow to orange (in methanol) or to red (in ether or DCM). When yellow crystals of **Ag_{14}-DMF** were dissolved in a solvent with a higher coordination power (such as DMSO, pyridine), the DMF molecules should be replaced, leading to a small changes in the optical spectrum and the resulting solution remains yellow in color.

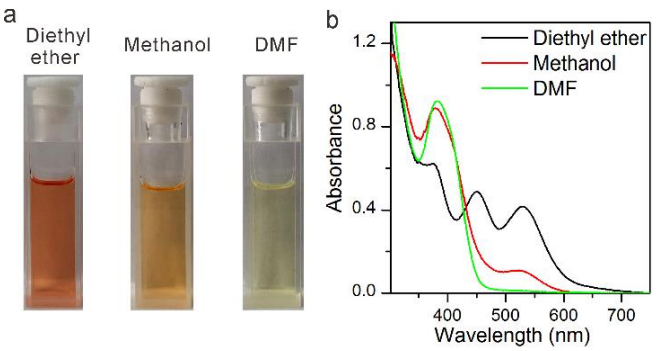

Figure 2. Photographs (a) and UV-vis spectra (b) of the crystals of **Ag_{14}-DMF** dissolved in diethyl ether, methanol and DMF solutions.

In order to verify our hypothesis, we dissolved the crystals of **Ag_{14}-DMF** in the mixed solution of diethyl ether and DCM and washed with water. Methanol, DMSO and pyridine were then added. The resulting solution mixtures were slowly evaporated to obtain the crystals with yield up to 95%. (See experimental section

10.1002/anie.202101141

for more details) SCXRD revealed that the obtained clusters formulated as $[Ag_{14}(SPh(CF_3)_2)_{12}(PPh_3)_4(CH_4O)_4]$ (**Ag_{14}-MeOH**), $[Ag_{14}(SPh(CF_3)_2)_{12}(PPh_3)_4(C_2H_6SO)_4]$ (**Ag_{14}-DMSO**) and $[Ag_{14}(SPh(CF_3)_2)_{12}(PPh_3)_4(C_5H_5N)_4]$ (**Ag_{14}-Py**), respectively. (Table S3, S4 and S5) The ^{1}H NMR spectra of the crystals of **Ag_{14}-MeOH**, **Ag_{14}-DMSO** and **Ag_{14}-Py** are shown in Figure S7, S8 and S9, respectively. As shown in Figure S10, the structures of **Ag_{14}-MeOH**, **Ag_{14}-DMSO** and **Ag_{14}-Py** are similar with **Ag_{14}-DMF** except that the four DMF molecules were replaced by four CH_3OH, DMSO or pyridine molecules, respectively. This observation implies that the four DMF ligands are only weakly bonded on the **Ag_{14}** cluster. Interestingly, the color of the crystals of **Ag_{14}-DMF** changed from yellow to dark red gradually when it was exposed to air, and it turned back to yellow again when DMF was added (Figure S11). This process is *completely reversible*. As shown in the ^{1}H NMR spectra of the crystals of **Ag_{14}-DMF** before and after air exposure (Figure S12), the peaks of DMF (8.02, 2.97, 2.97 ppm) almost disappeared after exposure to air, implying that the DMF molecules were readily dissociated. The solid state UV-vis spectrum of the red crystals remained the absorption peaks at the wavelengths similar to those for the ether solution of **Ag_{14}-DMF** (Figure S13), suggesting that DMF molecules were also dissociated from **Ag_{14}-DMF** when it was dissolved in diethyl ether. All these observations indicate that the DMF molecules in **Ag_{14}-DMF** are labile. It occurred to us that, given the weakly protected surface Ag sites, the **Ag_{14}** cluster should possess high surface reactivity.

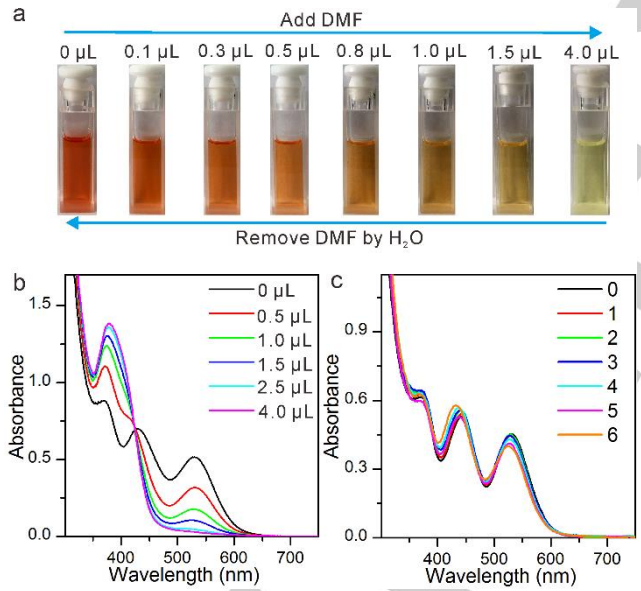

Figure 3. a) Photographs of the diethyl ether solution of **Ag_{14}-DMF** when adding different amount of DMF. b) UV-vis spectra variation of the diethyl ether solution of **Ag_{14}-DMF** when adding different amount of DMF. c) UV-vis spectra of **Ag_{14}-DMF** in diethyl ether after add-remove DMF in different cycles.

Modulating the optical properties of Ag_{14} cluster. The high surface reactivity of the DMF-Ag sites in **Ag_{14}-DMF** provides an opportunity to modulate the optical properties of **Ag_{14}** cluster through external stimuli. For instance, when DMF was added to diethyl ether solution of **Ag_{14}-DMF**, the color of the solution changed from pink to yellow rapidly. Due to the significantly different absorption profiles of the pink and light yellow solutions, the conversion process can be monitored by absorption and emission spectroscopy. As shown in Figure 3a, upon adding DMF, the color of the solution was changed from pink to light yellow gradually. The variation of the UV-vis spectra and fluorescent spectra are shown in Figure 3b and Figure S14, respectively. With the increase of DMF, the peak at 375 nm increased while the peaks at 527 and 450 nm disappeared concomitantly in the UV-vis spectra. In their fluorescent spectra, the red emission at 640 nm changed to yellow emission at 550 nm gradually. Moreover, this process is totally reversible. When DMF extracted from the diethyl ether solution by layering with water, the color of the solution was changed from light yellow to pink immediately, which can be recycled many times without intensity loss in the UV-vis spectra (Figure 3c). Other coordinative solvents can also be used to modulate the optical properties of **Ag_{14}**. According to the change of UV-vis spectra after adding the same amount of MeOH, DMSO, DMF and pyridine molecules to the diethyl ether solution of the crystals of **Ag_{14}-DMF**, the bond strength between different solvent molecules and **Ag_{14}** can be thus defined in the order of MeOH <DMF ~ DMSO <Py (Figure S15). These results suggest that it is possible to modulate the optical properties of a cluster based on the coordinating power of the solvent due to the high surface reactivity of the **Ag_{14}** cluster.

DFT calculations. In order to understand the reason why stimulation with DMF can result in the dramatic change in optical properties of **Ag_{14}**, we performed DFT calculations for the clusters in different conformations. We used the GPAW software with real-space grid (details are given in Computational Methods section). Structure relaxation confirmed that the experimental structures are stable local energy minimum structures. During the relaxation with the PBE-functional, the metal core expanded slightly but the overall structure remained otherwise intact. The differences in the coordination ability and strength of the weakly bound ligands (MeOH, DMF, DMSO, Py) were estimated with a full ligand exchange reaction, *e.g.,* **Ag_{14}-DMF** + 4Py > **Ag_{14}-Py** + 4DMF, in which the incoming and the detached ligands were treated as isolated molecules. By comparing energetics between all cluster pairs could be ordered from the strongest to the weakest binder as follows: 1) DMSO, 2) DMF, 3) Py and 4) MeOH. A list of all calculated energies is given in Table S6. The difference to the experimental result may be explained by the solvation energies which are missing in our calculations and would be difficult to calculate reliably with DFT.

The most important unrevealed observation relates to the change of optical spectrum when stimulating the **Ag_{14}-DMF** sample with DMF. Based on the hypothesis that the detachment of DMF creates a spectrum with three peaks whereas the intact **Ag_{14}-DMF** cluster shows only one main peak. To explain the experimental observations we formed a model structure by removing all weakly bound DMF-ligands from the surface and relaxed the system to the local minimum configuration. Calculated spectra in Figure S16 show two distinguished peaks at 471 nm and 335 nm for the intact cluster with DMF and three for the cluster without DMF-molecules at 473 nm, 384 nm and 331 nm. Surprisingly, the positions of the peaks are in good agreement with the experimentally measured spectrum for the latter, but the original **Ag_{14}-DMF** cluster has clear discrepancy at low energy spectrum. Note that the measured spectral series in Figure 3b show also a spectrum with two features, but at the higher

10.1002/anie.202101141

extremum of DMF addition the lowest energy peak at 527 nm finally vanishes.

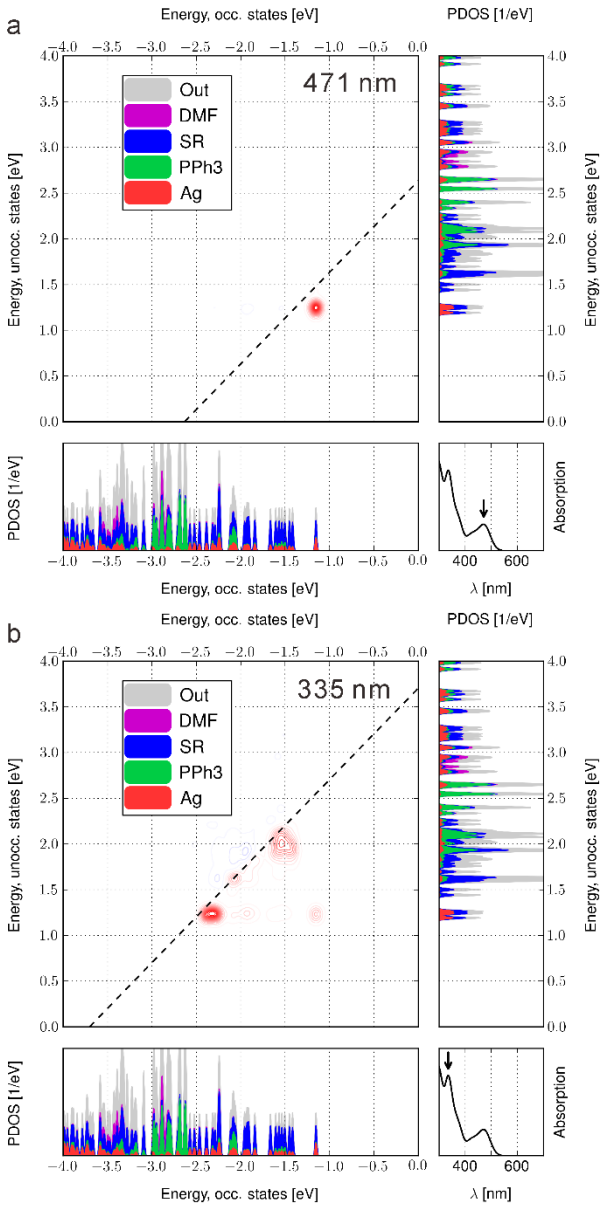

Figure 4. Dipole transition contribution map of **Ag_{14}-DMF** cluster: a) 471 nm; b) 335 nm. Contour plot top left corner shows the strengthening (in red) and screening (in blue) contributions to the transition dipole moment of the peak labeled in lower right corner optical spectrum. Lower left and top right panels shows the occupied and unoccupied Kohn-Sham states projected to different parts (DMF, thiolates=SR, phosphines=PPh_3 and silver=Ag) of the structure.

At this point the nature of the peaks is important to be clarified, for which time dependent perturbation theory was used. The analysis was done with so called dipole transition contribution maps visualizing the strengthening and screening excitations to the peaks in Kohn-Sham basis. Figure 4 and Figure S17 show clearly that in both studied clusters the lowest energy peaks are from HOMO to LUMO type of transitions. These states are localized to the metal core and correspond to 1S to 1P type of superatom transitions based on superatom electron state symmetries shown in Figure 5. Both of the states are well separated from the ligand states. At higher energies the ligands states start to contribute, the highest energy peak being solely from ligand-to-ligand type of transitions. States that are localized to DMF ligands are not involved in the contributions as they are localized further away from the Fermi energy and therefore is an underlying indirect effect to the structure that changes the lower energy spectrum under stimulation with DMF. Obviously, that change correlates with the changes in the superatom states.

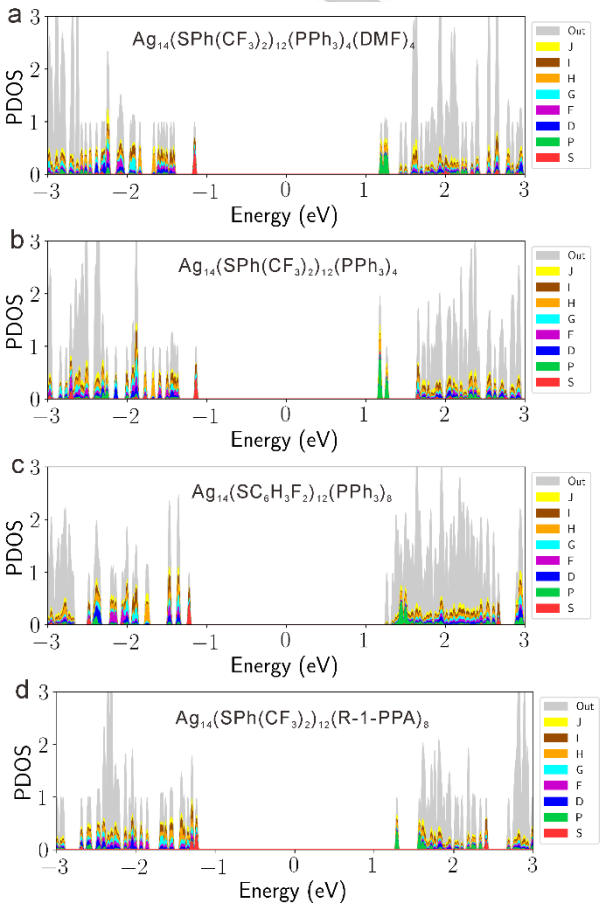

Figure 5. Electronic structure of **Ag_{14}** clusters with DMF in (a) and without DMF in (b) as a projection to spherical harmonics functions that denote the superatom state symmetries as labeled in figure. The same analysis is shown for [$Ag_{14}(SC_6H_3F_2)_{12}(PPh_3)_8$] cluster in (c) and for the chiral [$Ag_{14}(SPh(CF_3)_2)_{12}$(R-1-PPA)$_8$] cluster in (d).

For comparison we calculated the spectrum of the analogous, [$Ag_{14}(SC_6H_3F_2)_{12}(PPh_3)_8$].[12] All-phosphine cluster with the same level of theory which is shown in Figure S18. Calculations give only one clear peak in the spectrum at 415 nm. The reason can be seen from the electronic structure. For the all-phosphine cluster the HOMO-LUMO gap is 0.3 eV larger (2.65 eV) compared to the same of **Ag_{14}-DMF** cluster (2.35 eV). The HOMO-LUMO gap of **Ag_{14}** cluster without DMF was 2.31 eV. In addition the superatom 1S and 1P states are accompanied with the ligand states and not separated as shown in Figure 5c. As a consequence, the optical spectrum gets more monotonous regardless of the formation of one main peak which is still mostly caused by 1S to 1P type of transitions as visualized in Figure S19.

10.1002/anie.202101141

DFT Molecular Dynamics simulations. We performed molecular dynamics (MD) simulations for **Ag_{14}** clusters with and without DMF, using Langevin dynamics at room temperature in total for 7.5 ps and 8.6 ps, respectively. The structural evolution is shown in the SI-videos. No major deformations were seen in the structures by qualitative inspection. To reveal the effects of smaller deformations to the optical spectra, 8 snapshot structures were taken after thermalization (at 3.0 ps) approximately at each 300 steps. The spectra show rich variation in shape including everything between one and three distinguished peaks, see Figure S20. Interestingly, for the intact cluster with DMF ligands there are more spectra with single peak and cluster without DMF has more spectra with three peaks and lower energy features. The average spectra for the ensemble in Figure 6 confirm this qualitatively inspected difference. The result is close to the measured spectra and prominently different from the calculated result got for the static, crystal structure-based clusters. It can be further confirmed that during MD-simulation the HOMO-LUMO gap is on average larger for **Ag_{14}** cluster with DMF (2.00 eV) than without DMF (1.89 eV). The gap is lowered in both systems as compared to static structures but the relative difference in the gap is getting larger.

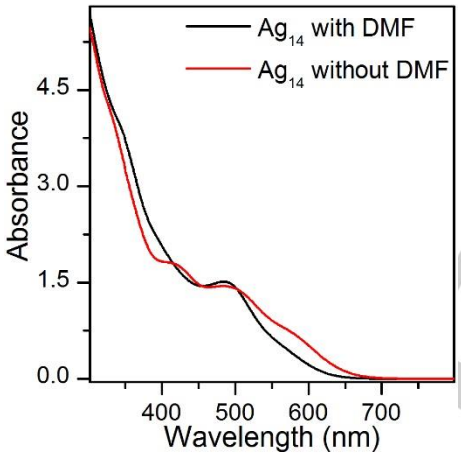

Figure 6. Ensemble-averaged optical absorption spectra of **Ag_{14}** cluster with and without DMF from DFT MD simulations.

Because the initial static **Ag_{14}-DMF** structure for MD-simulation was not supporting the experimental observation, it can be expected that the same qualitative behavior even with larger time scales and increased sampling. Obviously, the time scale used here is long enough to capture the required structure dynamics and deformations behind the observation. Nevertheless, considerable increase in the time scale and in the sampling would require significantly more computational resources.

Conversion of the racemic mixtures of Ag_{14}-DMF to homochiral Ag_{14} clusters. Based on the above observations, it occurred to us that chiral amines may be introduced to form optically pure chiral **Ag_{14}** clusters. As is well known, chiral amines are often used to modify nanoparticles for chirality-related applications.[14] However, it is often difficult to incorporate amine ligands on clusters due to the weak coordination ability of amines in comparison with thiolate, alkynyl, or phosphine ligands. The situation is different here. The high surface reactivity of **Ag_{14}-DMF** induced by bulky thiolate ligands described above provides an excellent opportunity to achieve this goal. In this work, R-1-phenylpropylamine (R-1-PPA) and S-1-phenylpropylamine (S-1-PPA), a pair of commercially available chiral amines, were chosen. These two enantiomeric amines exhibit two peaks at 243 and 291 nm, as mirror images, in the CD spectra (Figure S21). Here they were used to post-modify the ligand shell of **Ag_{14}-DMF** to form the corresponding enantiomeric pair of $[Ag_{14}(SPh(CF_3)_2)_{12}(R\text{-}1\text{-}PPA)_8]$ and $[Ag_{14}(SPh(CF_3)_2)_{12}(S\text{-}1\text{-}PPA)_8]$ (abbre. as **Ag_{14}-R-1-PPA** and **Ag_{14}-S-1-PPA**, respectively. Synthetic details can be found in the Experimental Section). To the best of our knowledge, the present work is the first time that chiral amines were incorporated into a silver cluster to realize chirality.

SCXRD revealed that the homochiral **Ag_{14}** clusters **Ag_{14}-R-1-PPA** and **Ag_{14}-S-1-PPA** crystallized in chiral space group (*C*2). (*cf.* Table S7 and S8) The high purity of the ^{1}H NMR spectra of the crystals of **Ag_{14}-S-1-PPA** indicates the homogeneity of the samples (Figure S22). As shown in Figure S23, the resulting enantiomeric clusters exhibit perfect mirror symmetry. The overall structures of **Ag_{14}-R/S-1-PPA** are similar to **Ag_{14}-DMF**, except the DMF and PPh_3 ligands in the outer shell of **Ag_{14}-DMF** were substituted by eight chiral amine ligands. Detailed analysis of the molecular structures of **Ag_{14}-DMF** revealed that, initially, the silver framework of this cluster conforms to an idealized O_h symmetry and is achiral. However, due to severe steric hindrance between the twelve bulky thiolate ligands and the eight chiral amines (or four PPh_3 and four DMF), the thiolate ligands of **Ag_{14}** clusters are heavily twisted, lowering the point-group symmetry to C_2 symmetry (Figure 7a, b) and the cluster becomes chiral. For **Ag_{14}-DMF**, the twisting directions are equally probable, thereby producing a racemate. For **Ag_{14}-R-1-PPA** and **Ag_{14}-S-1-PPA**, the chiral amine ligands induce the formation of optically pure chiral clusters. The degree of twisting of the sulfur, silver and nitrogen atoms can be measured as twist angles with reference to the Ag_6 core (viewed along the C_2 symmetry axis) (Figure S24) and the results are shown in Table S9.

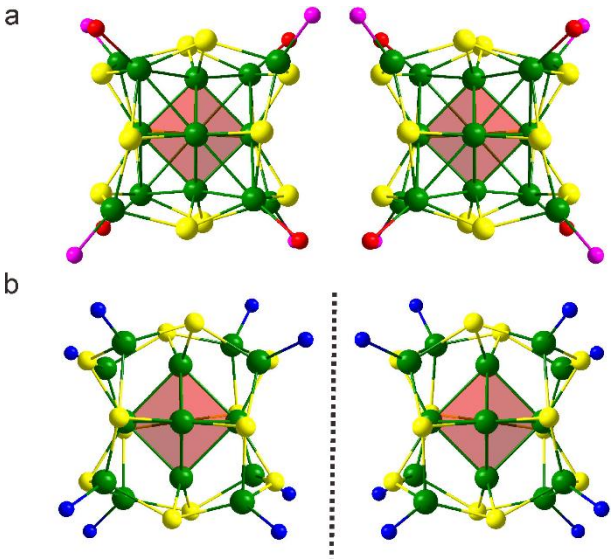

Figure 7. a) Core structures of the **Ag_{14}-DMF** enantiomer pair. b) Core structures of **Ag_{14}-R-1-PPA** (left) and **Ag_{14}-S-1-PPA** (right) Color legend: green sphere, Ag; yellow sphere, S; pink sphere, P; blue sphere, N; red sphere, O. [15]

As shown in Figure 8a, the UV-vis spectrum of **Ag_{14}-R-1-PPA** exhibit one strong band at 370 nm, which is slightly blue-shifted compared to the **Ag_{14}-DMF** in DMF (380 nm). Calculated optical absorption spectrum in Figure 8b shows two lower intensity features in range 375-500 nm and a steep increase below it, associated with a high energy feature at 325 nm. The circular dichroism (CD) spectra of the crystals of **Ag_{14}-R-1-PPA** and **Ag_{14}-S-1-PPA** in diethyl ether solution give perfect mirror images from 310 to 440 nm and two clear signals (minima or maxima: 340 and 375 nm) are observed. (Figure 8c) The calculated CD spectrum of **Ag_{14}-R-1-PPA** is in good agreement with the measured spectrum showing similar minimum and maximum signals at the studied wavelength range (Figures 8c and d). Positions of the calculated signals are seen at 325 nm and 360 nm. Apparently the mentioned lowering of the structural symmetry connects to the changes in the optical spectra similarly as in the non-chiral systems. But here the structural changes are driven by the assembly of chiral ligands on the surface of cluster and the structure is probably more rigid.

Interestingly, when the crystals of **Ag_{14}-S-1-PPA** were dissolved in 5.0 × 10^{-2} mmol/mL R-1-PPA diethyl ether solution, it will convert into **Ag_{14}-R-1-PPA**. These conversions have been confirmed by SCXRD and CD spectral evidence (Figure S25). These observations confirm the high surface reactivities of the **Ag_{14}** clusters that provide an excellent opportunity for reversible dynamic control of their physical and chemical properties.

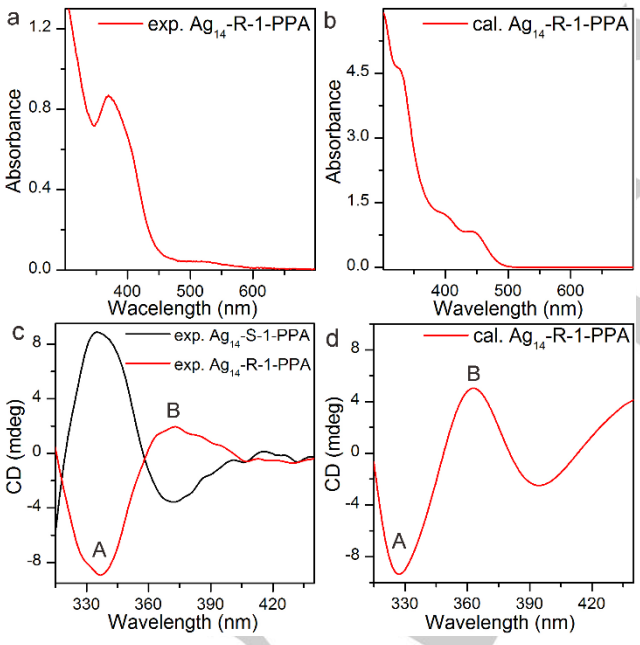

Figure 8. a) Experimental UV-vis spectrum of **Ag_{14}-R-1-PPA**. b) Calculated UV-vis spectrum of **Ag_{14}-R-1-PPA**. c) Experimental Circular dichroism (CD) spectra of the enantiomers of **Ag_{14}-R/S-1-PPA**. d) Calculated CD spectrum of **Ag_{14}-R-1-PPA**. Due to the dynamic nature of amine-Ag sites in solution, the crystals of **Ag_{14}-R/S-1-PPA** are dissolved in 2.0 × 10^{-2} mmol/mL R/S-1-PPA diethyl ether solution for optical spectra measurement. In panel (b) and (d) the most important peaks are labeled with A and B.

Conclusion

In conclusion, a silver cluster with weakly coordinated DMF ligands on the surface was synthesized through a large and small steric ligands mixed strategy. Through its high surface reactivities, we achieved modulating the optical properties of **Ag_{14}** cluster by removal or addition the DMF ligands. DFT calculations revealed that DMF ligands "on-off" on the silver sites changes the electron structure of **Ag_{14}** cluster, which further influence the optical properties. The best agreement to experiments is seen for dynamical ensemble of cluster structures which indicates the sensibility of the optical response to small deformations in structural symmetry of the cluster. Furthermore, chiral amine ligands (R/S-1-PPA) are successfully used to convert the racemic mixtures of **Ag_{14}-DMF** to homochiral **Ag_{14}** clusters. This is not only the first report of enantioselective conversion of racemic mixtures to homochiral clusters exhibiting 100% optical purity, but also opens the door for synthesis of atomic precise chiral clusters using chiral amine ligands. We believe the strategy for modulating the optical properties and generating chirality of metal clusters reported in this paper are useful in clusters design and chiral applications.

Acknowledgements

We thank the National Key R&D Program of China (2017YFA0207302), the NNSF of China (21890752, 21731005, 21721001), and the 111 Project (B08027) for financial support. The computational work at the University of Jyväskylä was supported by the Academy of Finland (grants 292352, 294217, 319208 and H.H.'s Academy Professorship). The computations were made at the Finnish Supercomputing Center CSC.

Conflict of interest

The authors declare no competing financial interest.

Keywords: Surface reactivities • chirality • circular dichroism • silver clusters • optical properties

[1] a) R. C. Jin, C. J. Zeng, M. Zhou, Y. X. Chen, *Chem. Rev.* **2016**, *116*, 10346-10413; b) I. Chakraborty, T. Pradeep, *Chem. Rev.* **2017**, *117*, 8208-8271; c) J. Z. Yan, B. K. Teo, N. F. Zheng, *Acc. Chem. Res.* **2018**, *51*, 3084-3093.

[2] a) Y. X. Du, H. T. Sheng, D. Astruc, M. Z. Zhu, *Chem. Rev.* **2019**, *120*, 526-622; b) X. Kang, M. Z. Zhu, *Chem. Soc. Rev.* **2019**, *48*, 2422-2457; c) B. Li, H. T. Fan, S. Q. Zang, H. Y. Li, L. Y. Wang, *Coordin. Chem. Rev.* **2018**, *377*, 307-329; d) Z. B. Gan, N. Xia, Z. K. Wu, *Acc. Chem. Res.* **2018**, *51*, 2774-2783; e) R. C. Jin, H. F. Qian, Z. K. Wu, Y. Zhu, M. Z. Zhu, A. Mohanty, N. Garg, *J. Phys. Chem. Lett.* **2010**, *1*, 2903-2910; f) Y. Yu, Z. T. Luo, Y. Yu, J. Y. Lee, J. P. Xie, *ACS Nano* **2012**, *6*, 7920-7927; g) S. Yang, J. S. Chai, Y. B. Song, J. Q. Fan, T. Chen, S. X. Wang, H. Z. Yu, X. W. Li, M. Z. Zhu, *J. Am. Chem. Soc.* **2017**, *139*, 5668-5671; h) Q. F. Yao, Y. Feng, V. Fung, Y. Yu, D. E. Jiang, J. Yang, J. P. Xie, *Nat. Commun.* **2017**, *8*, 1555; i) X. Kang, X. Wei, S. Jin, Q. Q. Yuan, X. Q. Luan, Y. Pei, S. X. Wang, M. Z. Zhu, R. C. Jin, *Proc. Natl. Acad. Sci. U.S.A.* **2019**, *116*, 18834-18840; j) Q. Li, T. Y. Luo, M. G. Taylor, S. X. Wang, X. F. Zhu, Y. B. Song, G. Mpourmpakis, N. L. Rosi, R. C. Jin, *Sci. Adv.* **2017**, *3*, e1603193.

[3] a) G. X. Chen, C. F. Xu, X. Q. Huang, J. Y. Ye, L. Gu, G. Li, Z. C. Tang, B. H. Wu, H. Y. Yang, Z. P. Zhao, Z. Y. Zhou, G. Fu, N. F. Zheng, *Nat. Mater.* **2016**, *15*, 564-569; b) R. L. Donkers, Y. B. Song, R. W. Murray, *Langmuir* **2004**, *20*, 4703-4707.

[4] a) H. Shen, G. C. Deng, S. Kaappa, T. D. Tan, Y. Z. Han, S. Malola, S. C. Lin, B. K. Teo, H. Häkkinen, N. F. Zheng, *Angew. Chem. Int. Ed.* **2019**,

58, 17731-17735; b) H. Shen, Z. Xu, M. S. A. Hazer, Q. Y. Wu, J. Peng, R. X. Qin, S. Malola, B. K. Teo, H. Häkkinen, N. F. Zheng, *Angew. Chem. Int. Ed.* **2021**, *60*, 3752-3758; c) L. T. Ren, P. Yuan, H. F. Su, S. Malola, S. C. Lin, Z. C. Tang, B. K. Teo, H. Häkkinen, L. S. Zheng, N. F. Zheng, *J. Am. Chem. Soc.* **2017**, *139*, 13288-13291.

[5] a) S. Knoppe, T. Burgi, *Acc. Chem. Res.* **2014**, *47*, 1318-1326; b) Y. Yang, X. L. Pei, Q. M. Wang, *J. Am. Chem. Soc.* **2013**, *135*, 16184-16191; c) D. Zerrouki, J. Baudry, D. Pine, P. Chaikin, J. Bibette, *Nature* **2008**, *455*, 380-382; d) J. Q. Wang, Z. J. Guan, W. D. Liu, Y. Yang, Q. M. Wang, *J. Am. Chem. Soc.* **2019**, *141*, 2384-2390; e) S. Malola, H. Häkkinen, *J. Am. Chem. Soc.* **2019**, *141*, 6006-6012.

[6] a) L. W. Liao, S. L. Zhuang, C. H. Yao, N. Yan, J. S. Chen, C. M. Wang, N. Xia, X. Liu, M. B. Li, L. L. Li, X. L. Bao, Z. K. Wu, *J. Am. Chem. Soc.* **2016**, *138*, 10425-10428; b) P. D. Jadzinsky, G. Calero, C. J. Ackerson, D. A. Bushnell, R. D. Kornberg, *Science* **2007**, *318*, 430-433; c) C. J. Zeng, Y. X. Chen, K. Kirschbaum, K. J. Lambright, R. C. Jin, *Science* **2016**, *354*, 1580-1584; d) M. S. Bootharaju, H. Chang, G. C. Deng, S. Malola, W. Baek, H. Hakkinen, N. F. Zheng, T. Hyeon, *J. Am. Chem. Soc.* **2019**, *141*, 8422-8425.

[7] a) I. Dolamic, S. Knoppe, A. Dass, T. Burgi, *Nat. Commun.* **2012**, *3*, 798; b) Y. F. Zhu, H. Wang, K. W. Wan, J. Guo, C. T. He, Y. Yu, L. Y. Zhao, Y. Zhang, J. W. Lv, L. Shi, R. X. Jin, X. X. Zhang, X. H. Shi, Z. H. Tang, *Angew. Chem. Int. Ed.* **2018**, *57*, 9059-9063; c) S. Knoppe, I. Dolamic, A. Dass, T. Burgi, *Angew. Chem. Int. Ed.* **2012**, *51*, 7589-7591.

[8] a) H. Y. Yang, J. Z. Yan, Y. Wang, G. C. Deng, H. F. Su, X. J. Zhao, C. F. Xu, B. K. Teo, N. F. Zheng, *J. Am. Chem. Soc.* **2017**, *139*, 16113-16116; b) G. C. Deng, S. Malola, J. Z. Yan, Y. Z. Han, P. Yuan, C. W. Zhao, X. T. Yuan, S. C. Lin, Z. C. Tang, B. K. Teo, H. Häkkinen, N. F. Zheng, *Angew. Chem. Int. Ed.* **2018**, *57*, 3421-3425; c) M. Sugiuchi, Y. Shichibu, K. Konishi, *Angew. Chem. Int. Ed.* **2018**, *57*, 7855-7859; d) M. M. Zhang, X. Y. Dong, Z. Y. Wang, H. Y. Li, S. J. Li, X. Zhao, S. Q. Zang, *Angew. Chem. Int. Ed.* **2019**, *59*, 10052-10058; e) S. Knoppe, O. A. Wong, S. Malola, H. Hakkinen, T. Burgi, T. Verbiest, C. J. Ackerson, *J. Am. Chem. Soc.* **2014**, *136*, 4129-4132; f) Y. Yang, Q. Zhang, Z. J. Guan, Z. A. Nan, J. Q. Wang, T. Jia, W. W. Zhan, *Inorg. Chem.* **2019**, *58*, 3670-3675; g) S. Takano, T. Tsukuda, *J. Phys. Chem. Lett.* **2016**, *7*, 4509-4513.

[9] a) Y. Yanagimoto, Y. Negishi, H. Fujihara, T. Tsukuda, *J. Phys. Chem. B* **2006**, *110*, 11611-11614; b) Y. N. Wang, B. Nieto-Ortega, T. Bürgi, *Nat. Commun.* **2020**, *11*, 4562.

[10] a) H. Shen, T. Mizuta, *Chem. -Eur. J.* **2017**, *12*, 2904-2907; b) S. S. Zhang, F. Alkan, H. F. Su, C. M. Aikens, C. H. Tung, D. Sun, *J. Am. Chem. Soc.* **2019**, *141*, 4460-4467.

[11] S. Li, X. S. Du, B. Li, J. Y. Wang, G. P. Li, G. G. Gao, S. Q. Zang, *J. Am. Chem. Soc.* **2018**, *140*, 594-597.

[12] H. Y. Yang, J. Lei, B. H. Wu, Y. Wang, M. Zhou, A. D. Xia, L. S. Zheng, N. F. Zheng, *Chem. Commun.* **2013**, *49*, 300-302.

[13] L. Falivene, Z. Cao, A. Petta, L. Serra, A. Poater, R. Oliva, V. Scarano, L. Cavallo, *Nat. Chem.* **2019**, *11*, 872–879.

[14] a) X. X. Zheng, L. Zhang, J. Y. Li, S. Z. Luo, J. P. Cheng, *Chem. Commun.* **2011**, *47*, 12325-12327; b) L. Deiana, Y. Jiang, C. Palo-Nieto, S. Afewerki, C. A. Incerti-Pradillos, O. Verho, C. W. Tai, E. V. Johnston, A. Córdova, *Angew. Chem. Int. Ed.* **2014**, *53*, 3447-3451; c) H. Yao, T. Fukui, K. Kimura, *J. Phys. Chem. C* **2008**, *112*, 16281–16285.

[15] Deposition Numbers 2054073 to 2054078 contain the supplementary crystallographic data for this paper. These data are provided free of charge by the joint Cambridge Crystallographic Data Centre and Fachinformationszentrum Karlsruhe Access Structures service.

10.1002/anie.202101141

Entry for the Table of Contents

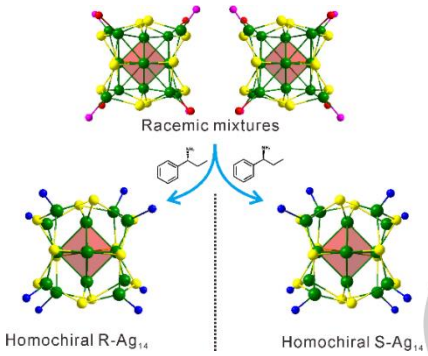

Bulky surface ligands greatly enhance the surface ligands reactivity of metal clusters, allowing easy modulation of their optical properties by reversible surface ligation. When chiral amines are introduced into the solution of racemic clusters, they are readily fully converted to optically pure homochiral clusters.